

# Dispersion-relation phase spectroscopy of intracellular transport

Ru Wang,<sup>1</sup> Zhuo Wang,<sup>2</sup> Larry Millet,<sup>3</sup> Martha U. Gillette,<sup>3</sup> A. J. Levine,<sup>4</sup> and Gabriel Popescu<sup>2,\*</sup>

<sup>1</sup>Quantitative Light Imaging Laboratory, Department of Mechanical and Science and Engineering, Beckman Institute for Advanced Science and Technology, University of Illinois at Urbana-Champaign, Urbana, Illinois 61801, USA

<sup>2</sup>Quantitative Light Imaging Laboratory, Department of Electrical and Computer Engineering, Beckman Institute for Advanced Science and Technology, University of Illinois at Urbana-Champaign, Urbana, Illinois 61801, USA

<sup>3</sup>Department of Cell and Developmental Biology, University of Illinois at Urbana-Champaign, Urbana Illinois 61801, USA

<sup>4</sup>Department of Chemistry & Biochemistry, University of California at Los Angeles, Los Angeles, California, USA

\*gpopescu@illinois.edu

**Abstract:** We used quantitative phase imaging to measure the dispersion relation, i.e. decay rate vs. spatial mode, associated with mass transport in live cells. This approach applies equally well to both discrete and continuous mass distributions without the need for particle tracking. From the quadratic experimental curve specific to diffusion, we extracted the diffusion coefficient as the only fitting parameter. The linear portion of the dispersion relation reveals the deterministic component of the intracellular transport. Our data show a universal behavior where the intracellular transport is diffusive at small scales and deterministic at large scales. Measurements by our method and particle tracking show that, on average, the mass transport in the nucleus is slower than in the cytoplasm.

©2010 Optical Society of America

**OCIS codes:** (180.0180) Microscopy ;(170.0170) Medical optics and biotechnology; (000.2700) General science.

---

## References and links

1. R. B. Vallee and M. P. Sheetz, "Targeting of motor proteins," *Science* **271**(5255), 1539–1544 (1996).
2. F. C. MacKintosh and C. F. Schmidt, "Active cellular materials," *Curr. Opin. Cell Biol.* **22**(1), 29–35 (2010).
3. C. P. Brangwynne, G. H. Koenderink, F. C. MacKintosh, and D. A. Weitz, "Cytoplasmic diffusion: molecular motors mix it up," *J. Cell Biol.* **183**(4), 583–587 (2008).
4. C. P. Brangwynne, G. H. Koenderink, F. C. MacKintosh, and D. A. Weitz, "Intracellular transport by active diffusion," *Trends Cell Biol.* **19**(9), 423–427 (2009).
5. A. Yildiz, J. N. Forkey, S. A. McKinney, T. Ha, Y. E. Goldman, and P. R. Selvin, "Myosin V walks hand-over-hand: single fluorophore imaging with 1.5-nm localization," *Science* **300**(5628), 2061–2065 (2003).
6. X. Trepat, L. H. Deng, S. S. An, D. Navajas, D. J. Tschumperlin, W. T. Gerthoffer, J. P. Butler, and J. J. Fredberg, "Universal physical responses to stretch in the living cell," *Nature* **447**, 592–595 (2007).
7. B. Fabry, G. N. Maksym, J. P. Butler, M. Glogauer, D. Navajas, and J. J. Fredberg, "Scaling the microrheology of living cells," *Phys. Rev. Lett.* **87**(14), 148102 (2001).
8. A. Caspi, R. Granek, and M. Elbaum, "Enhanced diffusion in active intracellular transport," *Phys. Rev. Lett.* **85**(26), 5655–5658 (2000).
9. D. Mizuno, C. Tardin, C. F. Schmidt, and F. C. Mackintosh, "Nonequilibrium mechanics of active cytoskeletal networks," *Science* **315**(5810), 370–373 (2007).
10. B. Wang, S. M. Anthony, S. C. Bae, and S. Granick, "Anomalous yet Brownian," *Proc. Natl. Acad. Sci. U.S.A.* **106**(36), 15160–15164 (2009).
11. C. P. Brangwynne, G. H. Koenderink, F. C. MacKintosh, and D. A. Weitz, "Nonequilibrium microtubule fluctuations in a model cytoskeleton," *Phys. Rev. Lett.* **100**, 118104 (2008).
12. G. Popescu, in *Methods in Cell Biology*, 87–115, ed. Jena, B. P.), Academic Press, San Diego, 2008.
13. Y. K. Park, C. A. Best, T. Auth, N. S. Gov, S. A. Safran, G. Popescu, S. Suresh, and M. S. Feld, "Metabolic remodeling of the human red blood cell membrane," *Proc. Natl. Acad. Sci. U.S.A.* **107**(4), 1289–1294 (2010).
14. Y. K. Park, M. Diez-Silva, G. Popescu, G. Lykotrafitis, W. Choi, M. S. Feld, and S. Suresh, "Refractive index maps and membrane dynamics of human red blood cells parasitized by *Plasmodium falciparum*," *Proc. Natl. Acad. Sci. U.S.A.* **105**(37), 13730–13735 (2008).
15. G. Popescu, T. Ikeda, K. Goda, C. A. Best-Popescu, M. Laposata, S. Manley, R. R. Dasari, K. Badizadegan, and m. S. Feld, "Optical measurement of cell membrane tension," *Phys. Rev. Lett.* **97**(21), 218101 (2006).

16. Y. K. Park, C. A. Best, K. Badizadegan, R. R. Dasari, M. S. Feld, T. Kuriabova, M. L. Henle, A. J. Levine, and G. Popescu, "Measurement of red blood cell mechanics during morphological changes," *Proc. Natl. Acad. Sci. U.S.A.* **107**(15), 6731–6736 (2010).
17. G. Popescu, Y. Park, W. Choi, R. R. Dasari, M. S. Feld, and K. Badizadegan, "Imaging red blood cell dynamics by quantitative phase microscopy," *Blood Cells Mol. Dis.* **41**(1), 10–16 (2008).
18. Z. Wang, L. J. Millet, M. Mir, H. Ding, S. Unarunotai, J. A. Rogers, M. U. Gillette, and G. Popescu, "Spatial light interference microscopy (SLIM)," *Opt. Express* **19**(2), 1016–1026 (2011).
19. F. Zernike, "How I discovered phase contrast," *Science* **121**(3141), 345–349 (1955).
20. H. F. Ding, Z. Wang, F. Nguyen, S. A. Boppart, and G. Popescu, "Fourier transform light scattering of inhomogeneous and dynamic structures," *Phys. Rev. Lett.* **101**(23), 238102 (2008).
21. Z. Wang, I. S. Chun, X. L. Li, Z. Y. Ong, E. Pop, L. Millet, M. Gillette, and G. Popescu, "Topography and refractometry of nanostructures using spatial light interference microscopy," *Opt. Lett.* **35**(2), 208–210 (2010).
22. G. Popescu, Y. Park, N. Lue, C. Best-Popescu, L. Deflores, R. R. Dasari, M. S. Feld, and K. Badizadegan, "Optical imaging of cell mass and growth dynamics," *Am. J. Physiol. Cell Physiol.* **295**(2), C538–C544 (2008).
23. R. B. Bird, W. E. Stewart, and E. N. Lightfoot, *Transport Phenomena* (John Wiley & Sons, 1960).
24. B. J. Berne and R. Pecora, *Dynamic Light Scattering with Applications to Chemistry, Biology and Physics* (Wiley, 1976).
25. D. L. Coy, M. Wagenbach, and J. Howard, "Kinesin takes one 8-nm step for each ATP that it hydrolyzes," *J. Biol. Chem.* **274**(6), 3667–3671 (1999).
26. I. F. Sbalzarini and P. Koumoutsakos, "Feature point tracking and trajectory analysis for video imaging in cell biology," *J. Struct. Biol.* **151**(2), 182–195 (2005).
27. R. Wang, Z. Wang, J. Leigh, N. Sobh, L. Millet, M. U. Gillette, A. J. Levine, and G. Popescu, "One-dimensional deterministic transport in neurons measured by dispersion-relation phase spectroscopy," *J. Phys. Condens. Matter* **23**(37), 374107 (2011).
28. M. A. Thompson, J. M. Casolari, M. Badieirostami, P. O. Brown, and W. E. Moerner, "Three-dimensional tracking of single mRNA particles in *Saccharomyces cerevisiae* using a double-helix point spread function," *Proc. Natl. Acad. Sci. U.S.A.* **107**(42), 17864–17871 (2010).
29. Y. Tseng, J. S. Lee, T. P. Kole, I. Jiang, and D. Wirtz, "Micro-organization and visco-elasticity of the interphase nucleus revealed by particle nanotracking," *J. Cell Sci.* **117**(10), 2159–2167 (2004).
30. P. Marquet, B. Rappaz, P. J. Magistretti, E. Cuche, Y. Emery, T. Colomb, and C. Depeursinge, "Digital holographic microscopy: a noninvasive contrast imaging technique allowing quantitative visualization of living cells with subwavelength axial accuracy," *Opt. Lett.* **30**(5), 468–470 (2005).
31. J. Frank, S. Altmeyer, and G. Wernicke, "Non-interferometric, non-iterative phase retrieval by Green's functions," *J. Opt. Soc. Am. A* **27**(10), 2244–2251 (2010).
32. P. Bon, G. Maucort, B. Wattellier, and S. Monneret, "Quadriwave lateral shearing interferometry for quantitative phase microscopy of living cells," *Opt. Express* **17**(15), 13080–13094 (2009).

## 1. Introduction

Cells have developed a complex system to govern the internal transport of materials from single molecules to large complexes such as organelles during cell division [1]. While these processes are essential for the maintenance of cellular functions, their physical understanding is incomplete. It is now well documented that intracellular transport is mediated by both thermal diffusion and molecular motors that drive the cellular material out of equilibrium [2–4]. Measurements of the molecular motor driven transport have been made in the past via single molecule tracking (see e.g [5]). However, developing a more global picture of the spatial and temporal distribution of active transport in living cells remains an unsolved problem. Approaching this question experimentally can be reduced fundamentally to the problem of quantifying spatially heterogeneous dynamics at the microscopic scale. In the past, cellular material has been studied successfully by both externally-driven [6, 7] and passive particle tracking [8–10]. Recently, bending fluctuations of microtubules have been used to probe the active dynamics in actin networks [11].

In this article we introduce another approach – quantitative phase imaging (QPI) – to study the spatial and temporal distribution of active (deterministic) and passive (i.e. diffusive) transport processes in living cells. QPI reveals the optical pathlength distribution,  $s(\mathbf{r})$ , associated with the transmitted field through thin specimens, including live cells, (for a review, see [12]),

$$s(\mathbf{r}, t) = h(\mathbf{r}, t)n(\mathbf{r}, t) \quad (1)$$

In Eq. (1),  $h$  is the local thickness,  $\mathbf{r} = (x, y)$ , and  $n$  the refractive index contrast with respect to that of the surrounding medium. The pathlength fluctuations can be expressed to the first order as

$$\begin{aligned}
\Delta s(\mathbf{r}, t) &= s(\mathbf{r}, t) - \langle s(\mathbf{r}, t) \rangle_{\mathbf{r}, t} \\
&= \left[ \langle h(\mathbf{r}, t) \rangle_{\mathbf{r}, t} + \Delta h(\mathbf{r}, t) \right] \left[ \langle n(\mathbf{r}, t) \rangle_{\mathbf{r}, t} + \Delta n(\mathbf{r}, t) \right] - \langle h(\mathbf{r}, t) \rangle_{\mathbf{r}, t} \langle n(\mathbf{r}, t) \rangle_{\mathbf{r}, t} \quad (2) \\
&\simeq \langle n(\mathbf{r}, t) \rangle_{\mathbf{r}, t} \Delta h(\mathbf{r}, t) + \langle h(\mathbf{r}, t) \rangle_{\mathbf{r}, t} \Delta n(\mathbf{r}, t)
\end{aligned}$$

where the angular brackets indicate both temporal and spatial average. Thus,  $\Delta s(\mathbf{r}, t)$ , contains information about both out-of-plane thickness fluctuations,  $\Delta h$ , and in-plane refractive index fluctuations,  $\Delta n$ . Recently, the h-contribution to out-of-plane pathlength fluctuations has revealed new behavior in red blood cells, where  $n$  is well approximated by a constant [13–17]. Here we focus on the last term of Eq. (3), i.e., the in-plane mass transport revealed by  $\Delta n$ .

## 2. Spatial light interference microscopy (SLIM)

Experimentally, we employed a novel method recently developed in our laboratory, referred to as spatial light interference microscopy (SLIM) [18]. This imaging technique uses spatially coherent, broadband light, as illustrated in Fig. 1a. SLIM operates by adding spatial modulation to the image field of a commercial phase contrast microscope. In addition to the conventional  $\pi/2$  shift introduced between the scattered and unscattered light in phase contrast microscopy [19], we generated further phase shifts in increments of  $\pi/2$ . This additional modulation was achieved by using a liquid crystal phase modulator placed in the Fourier plane of the imaging field. In this setup, four images corresponding to each phase shift ( $n\pi/2$ ,  $n = 0, 1, 2, 3$ ) are recorded, to produce a quantitative phase image that is uniquely determined.

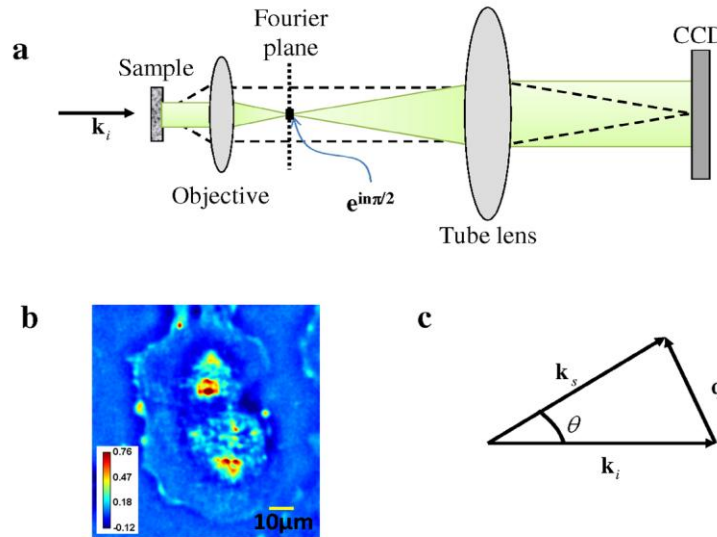


Fig. 1. a) Microscope as a scattering instrument: dash line, scattered field; green, unscattered fields. b) Quantitative phase image of a live cell. Color bar indicates phase in radians. c) Momentum transfer in a microscope.

Figure 1b depicts the quantitative phase image associated with a live cell. Note that, due to contrast changes induced by the four phase shifts, SLIM is able to minimize the effect of the well-known halo artifact that otherwise disturbs most phase contrast images. Recently, we have shown that the data contained in a quantitative phase image is equivalent to that of an extremely sensitive light scattering measurement [20], as shown in Fig. 1c. Thus,  $k_i$  is the

incident wave vector,  $k_s$  scattering wave vector, and  $q$  is momentum transfer (or scattering wavevector), which corresponds to a single spatial frequency in the image. The scattering angle (or momentum transfer) is limited only by the numerical aperture of the objective. Thus, QPI essentially allows measurements throughout the entire forward scattering half space from a single CCD exposure.

### 3. Dispersion-relation Phase Spectroscopy (DPS)

#### 3.1 Principle

Due to its broadband illumination, SLIM lacks speckle-induced noise and, thus, is highly sensitive to pathlength changes down to a fraction of nanometer [18, 21]. Throughout our measurements, the phase image acquisition rate was approximately 1 frame/s, which is lower than the decay rates associated with the bending and tension modes of tensed membrane fluctuations [15], such that we can safely ignore these contributions. The measured pathlength fluctuations in this case report on the dry mass transport within the cell [22]. This 2D dry mass density,  $\rho \propto \Delta n$ , satisfies an advection-diffusion equation, which includes both directed and diffusive transport [23],

$$D\nabla^2 \rho(\mathbf{r}, t) - \mathbf{v} \cdot \nabla \rho(\mathbf{r}, t) - \frac{\partial}{\partial t} \rho(\mathbf{r}, t) = 0, \quad (3)$$

where  $D$  is the diffusion coefficient of the particles and  $\mathbf{v}$  is the advection velocity due to flows in the sample cell. The spatiotemporal autocorrelation function of  $\rho$  is defined as

$$g(\mathbf{r}', \tau) = \langle \rho(\mathbf{r}, t) \rho(\mathbf{r} + \mathbf{r}', t + \tau) \rangle_{t, r}, \quad (4)$$

where the angular brackets indicate temporal and spatial average. In equation [4],  $\tau$  denotes the time difference. Taking the spatial Fourier transform of Eq. (4), we obtain the temporal autocorrelation,  $g$ , for each spatial mode  $q$ , as

$$g(\mathbf{q}, \tau) = e^{i\mathbf{q} \cdot \mathbf{v} \tau - Dq^2 \tau} \quad (5)$$

Equation (5) relates the measured temporal autocorrelation function to the diffusion coefficient,  $D$ , and velocity,  $v$ , of the matter in the cell. Note that the same autocorrelation can be measured via dynamic light scattering at a fixed scattering angle [24]. The experimental data, however, is averaged over a broad distribution of advection velocities, so that we may write the advection-velocity-averaged autocorrelation function as

$$\begin{aligned} g(\mathbf{q}, \tau) &= \left\langle e^{i\mathbf{v} \cdot \mathbf{q} \tau - Dq^2 \tau} \right\rangle_{\mathbf{v}} \\ &= e^{-Dq^2 \tau} \int P(|\mathbf{v} - \mathbf{v}_0|) e^{i\mathbf{v} \cdot \mathbf{q} \tau} d^2 \mathbf{v} \end{aligned} \quad (6)$$

where the probability distribution  $P$  of local advection velocities remains to be determined. In order to gain insight into the local distribution of advection speeds, we note that maximal kinesin speeds are approximately  $v = 0.8 \mu\text{m/s}$  [25]. Given the varying loads on such motors, we expect that the typical advection speeds will be distributed below this limit. The average advection speed may in fact be significantly lower than this value as there must be transport in a variety of directions. Consequently, we propose that  $P(v)$  is a Lorentzian of width  $\Delta v$  and that the mean advection velocity averaged over the scattering volume is significantly smaller than this velocity,  $v_0 \ll \Delta v$ . From this simple model we find that the integral in Eq. (6) can be evaluated as

$$g(\mathbf{q}, \tau) = e^{i\mathbf{v}_0 \cdot \mathbf{q} \tau} e^{-q \Delta v \tau - Dq^2 \tau}. \quad (7)$$

Thus, the mean advection velocity produces a modulation of frequency  $\omega(\mathbf{q}) = \mathbf{v}_0 \cdot \mathbf{q}$  to the temporal autocorrelation, which decays exponentially at a rate  $\Gamma(q) = \Delta v q + Dq^2$ . This relationship between the decay rate  $\Gamma$  and its wavenumber  $q$  represents the dispersion relation associated with intracellular transport. Thus, we refer to our method for studying transport as dispersion-relation phase spectroscopy (DPS), not to be confused with optical dispersion. We note that here “spectroscopy” refers to measuring spatiotemporal frequencies associated with mass transport and should not be confused with optical spectroscopy.

### 3.2 DPS validation with polystyrene microspheres in Brownian motion

In order to mimic better the viscous properties of the intracellular environment, we used SLIM to image the Brownian motion of 1  $\mu\text{m}$  polystyrene spheres in highly concentrated (99%) glycerol.

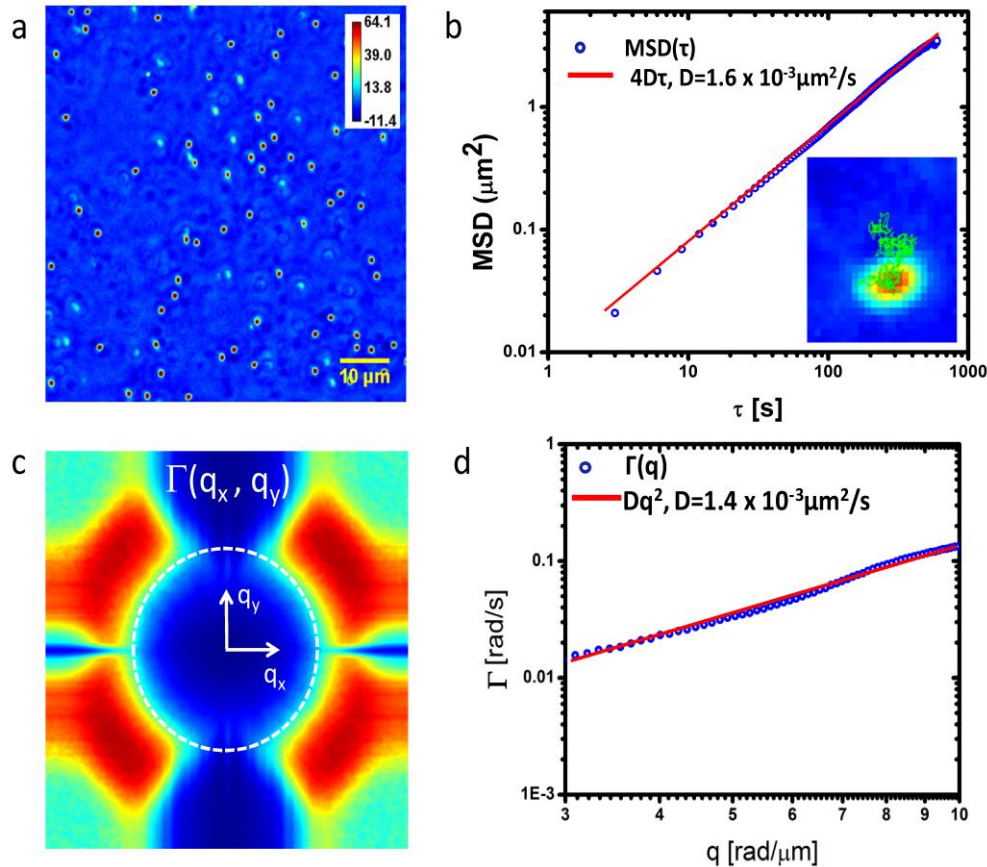


Fig. 2. a) Quantitative phase image of 1  $\mu\text{m}$  polystyrene beads in glycerol. Colorbar indicates pathlength in nm. b) Mean squared displacements (MSD) obtained by tracking individual beads in a. The inset illustrates the trajectory of a single bead. c) Decay rate vs. spatial mode,  $\Gamma(\mathbf{q})$ , associated with the beads in a. The dash ring indicates the maximum  $q$  values allowed by the resolution limit of the microscope. d) Azimuthal average of data in c) to yield  $\Gamma(q)$ . The fits with the quadratic function yields the value of the diffusion coefficient as indicated.

Figure 2a) shows the SLIM phase image of the sample with a field of view of  $73 \times 73 \mu\text{m}^2$ . We acquired SLIM images for 10 minutes with an acquisition rate of 1 frame/s. In principle the expected diffusion coefficient can be calculated via the Stokes-Einstein equation, provided the viscosity of glycerol is known. However, since the viscosity of concentrated glycerol is highly sensitive to the absolute value of the concentration, which is prone to experimental

(mixing) errors, instead we measured the diffusion coefficient by tracking individual particles in the phase image. Figure 2b shows the mean-squared displacements (MSD) obtained by averaging the trajectories of 54 particles. We used a numerical algorithm developed in Ref [26], and implemented in ImageJ by Levy. The linear fit yields  $D = (1.60 \pm 0.04) \times 10^{-3} \mu\text{m}^2/\text{s}$ . From the SLIM data, we calculated the dispersion relation,  $\Gamma(q_x, q_y)$ , as shown in Fig. 2c. Thus, we first perform the spatial Fourier transform of each frame, then calculated the temporal bandwidth,  $\Gamma$ , at each spatial frequency  $(q_x, q_y)$  through performing the temporal Fourier transform. We then perform the azimuthal average to obtain the radial function  $\Gamma(q)$ ,  $q = \sqrt{q_x^2 + q_y^2}$ . This experimental curve exhibits the expected  $q^2$  dependence, as illustrated in the log-log plot of Fig. 2d. The diffusion coefficient obtained is  $D = (1.40 \pm 0.07) \times 10^{-3} \mu\text{m}^2/\text{s}$  and compare very well with those measured via particle tracking.

Note that measuring diffusion via DPS eliminates the need for tracking individual particles and, more importantly, applies to particles that are not resolved in the image, i.e. are smaller than the diffraction spot of the microscope, as long as the particles travel over distances larger than the diffraction spot. This is largely the case in studying mass transport in live cells.

#### 4. DPS of live cells

We performed experiments on various types of live cells including glia and microglia cells, which are common in the central nervous system. In these cells, individual, un-labeled particles cannot be easily resolved or tracked by light microscopy. The cells were imaged in culture medium under physiological conditions, 37 °C and 5% CO<sub>2</sub> controls. All images were acquired with objective 40X/NA = 0.75 except Fig. 3e) where 63x/NA = 1.4 was used. Figure 3 shows results obtained on live cells. The cell-averaged  $\Gamma(q)$  curve shown in Fig. 3a-b exhibits a dominant quadratic shape, which yields a diffusion coefficient  $D = (9.60 \pm 0.04) \times 10^{-4} \mu\text{m}^2/\text{s}$ . Further, at the low-wavenumber end of the measurement range, we found a distinct linear dependence. From the linear term in fitting the dispersion curve, we extracted the advection velocity distribution width, obtaining a value of  $\Delta v = 1.3 \text{ nm/s}$ . Examining the data from live cells we note that we do not observe sinusoidal oscillations of the autocorrelation function, which would indicate a dominant velocity. This sets an upper limit on the mean advection velocity  $v_0 q_{\text{max}} \tau_{\text{max}} \ll 1$ . Given an observation time of ten minutes, the upper limit on the mean advection speed is  $\approx 0.1 \text{ nm/s}$  suggesting that, if present, a mean velocity is below this value. Thus, we can conclude that there are no persistent currents in the cell in steady-state. Deviations from the simple quadratic dispersion relation, however, demonstrate the presence of local directed transport, but this directed transport does not generate coherent flows within the cell. These results are fairly insensitive to the exact form of the advection speed distribution postulated. To obtain a part of the decay rate that is linear in the wave number term, one needs only postulate an upper speed cutoff and a reasonably broad distribution of speeds below this limit.

Further, we used DPS to study the mass transport in subcellular sub-domains. Figures 3c-h shows the SLIM images of various cells in culture and the  $\Gamma(q)$  curves associated with the respective regions. Note that the signal from the strips is associated with fluctuations along a single row of pixels, which explains the relatively higher noise level. These data exhibit a diversity of behavior, from purely diffusive in the microglia culture (Figs. 3c-d) to purely directed, in the putative dendrite of a neuron (Figs. 3e-f) [27].

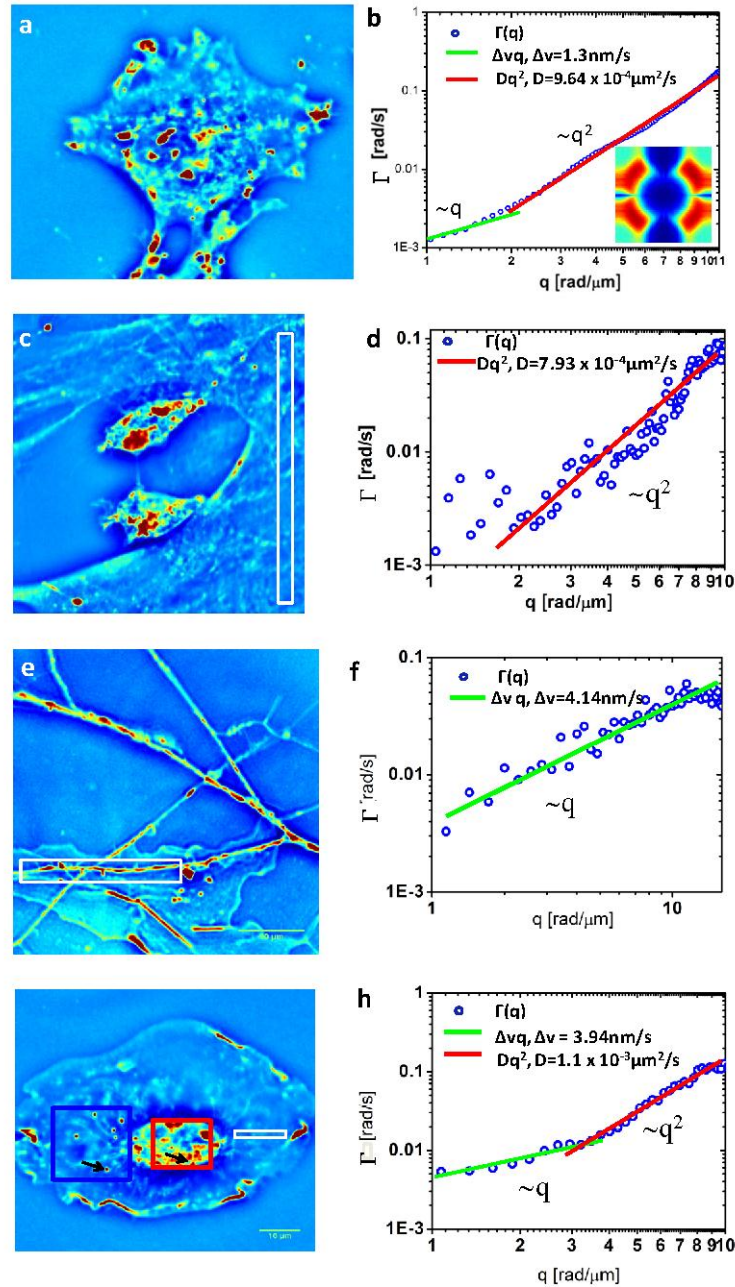


Fig. 3. Quantitative phase image of a culture of glia (a, g), microglia (c) and hippocampal neurons (e). b) Dispersion curve measured for the cell in a. The green and red lines indicate directed motion and diffusion, respectively, with the results of the fit as indicated in the legend. Inset shows the  $\Gamma(q_x, q_y)$  map. d, f, h) Dispersion curves,  $\Gamma(q)$ , associated with the white box regions in c, e) and g), respectively. The corresponding fits and resulting  $D$  and  $\Delta v$  values are indicated.

The entirely directed transport measured along the dendrite is in line with what is generally known about that ATP-consuming cargo transfer along microtubules via protein motors. Examining a narrow strip whose long axis is oriented radially with respect to the cell nucleus (Figs. 3g-h), we found that the transport is diffusive at short scales (below

approximately  $2\pi/q = 2 \mu\text{m}$ ) and directed at large scales. These findings suggest that, in general, both  $D$  and  $\Delta v$  may be inhomogeneous and anisotropic. Remarkably, the diffusion coefficients measured in the cell have much lower values than, for example, those associated with submicron particles in water. In order to study further this behavior, we performed a comparison between particle tracking and DPS measurements in both the nucleus and cytoplasm, as summarized in Fig. 4. Using the ImageJ “particle tracker” plugin [26], we tracked the mass centroid of 6 microdomains in the nucleus and the resulting averaged MSD is shown in Fig. 4a. Interestingly, the curve indicates a strong diffusive component that appears to have two modes, characterized by slightly different diffusion coefficients of  $0.88 \mu\text{m}^2/\text{s}$  and  $0.55 \mu\text{m}^2/\text{s}$ . Remarkably, the value obtained by DPS is  $0.6 \mu\text{m}^2/\text{s}$ , in between the two values given by tracking (Fig. 4b). The directed motion component of the MSD in Fig. 4a is seen more clearly for one domain in the inset. The value obtained is  $\Delta v = 2.8 \text{ nm/s}$ , while DPS yields  $\Delta v = 4.1 \text{ nm/s}$ .

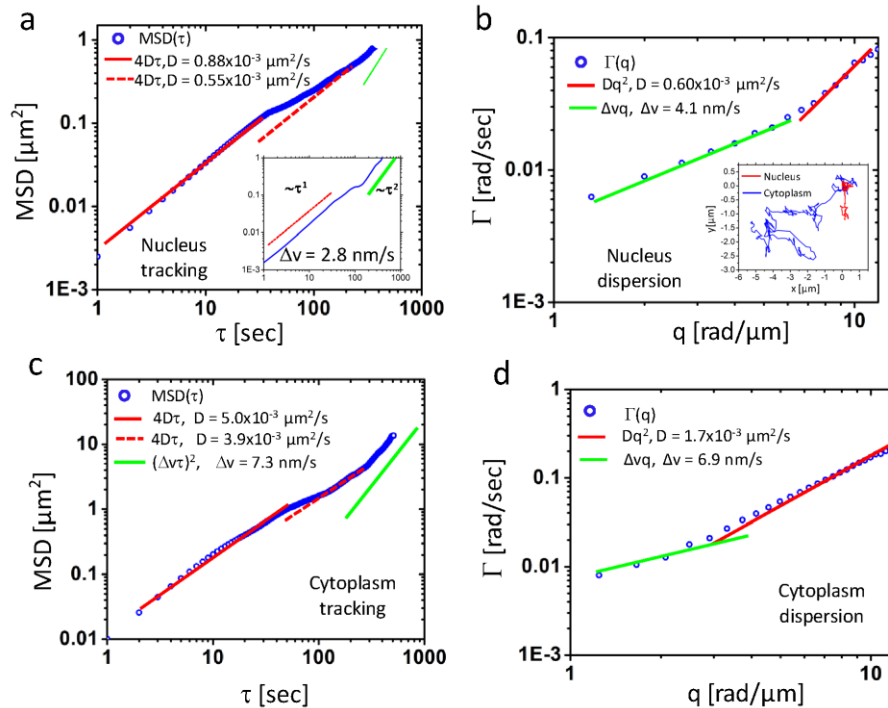


Fig. 4. a) and c) MSD ensemble-averaged over 7 and 6 particles in nucleus and cytoplasm regions, respectively, as indicated in Fig. 3g by the red and blue boxes. Corresponding fits give diffusion coefficients and standard deviation of drift velocity. Inset in a) shows the MSD for a particle in **log** scale where directed motion is indicated by green line. b) and d) are dispersion curves for the same area of a) and c. Inset are trajectories of two particles denoted by black arrow in Fig. 3g). The blue one is the particle at cytoplasm and red one is inside nucleus.

Tracking discrete particles in the cytoplasm results in higher diffusion coefficients than obtained by DPS,  $4\text{--}5 \mu\text{m}^2/\text{s}$  vs.  $1.7 \mu\text{m}^2/\text{s}$ , indicating that the continuous mass included in the DPS analysis is slower than the individual discrete particles. Interestingly, the width of the velocity distribution from DPS,  $\sim 6.9 \text{ nm/s}$ , as shown in Fig. 4d) is comparable with the average speed from particle tracking,  $\sim 7 \text{ nm/s}$ , as shown in Fig. 4c) which is expected from a system of particles actively transported in all directions isotropically. Our simultaneous measurements of DPS and particle tracking confirm that transport in continuous mass distributions is generally slower than that of discrete particles. This is the origin of the very low average values of the diffusion coefficients reported by DPS. Previous reports, by Thompson et al. [28] and Tseng et al. [29] reported similar values for the nuclear material. In

particular, Tseng et.al. obtained values of up to 520 Poise for the mean shear viscosity of the intranuclear region in Swiss 3T3 fibroblasts, while the values of the diffusion coefficient obtained by particle tracking match ours very well (of the order of  $10^{-3} \mu\text{m}^2/\text{s}$  and below). Interestingly, evidence was found for elastic behavior in nuclei at time scales below 1 s, which is currently not covered by our current instrument. Taken together, these results and ours indicate that the transport in live cells is far from being fully understood. We believe our dispersion relation analysis may provide a complementary approach for studying this phenomenon label-free, over broad spatial and temporal scales.

## 5. Summary and discussion

In sum, we developed an approach to study the intracellular transport that is based on measuring the dispersion curves,  $\Gamma(q)$ , from quantitative phase imaging. On average the mass transport in a live cell is diffusive at small scales (1  $\mu\text{m}$  and below) and deterministic at large scales (several microns). Our experiments show that continuous or completely transparent systems can be studied successfully by this method, in a label-free manner. Biologically, this result is quite reasonable: mass transport at large scales cannot be accomplished effectively by diffusion alone, as it is too slow; thus, it requires energy consumption. For example, neurons are a particular cell type that must accomplish transport over very large distances. Our results showing that the dendritic transport is largely directed strongly supports this idea.

It is worth noting that DPS can be equally used with other quantitative phase imaging techniques, such as these described recently in Refs [30–32]. The temporal limitations of studying subcellular transport are due to the acquisition rate; currently SLIM acquire 2.3 frames/s. However, this is not a limitation of principle and higher acquisition rates can be reached by using, for example, faster camera and spatial light modulation.

## Acknowledgments

This research was supported by National Science Foundation (CBET 08-46660 CAREER, CBET-1040462 MRI) and Grainger Foundation (G. Popescu). L. J. Millet was supported by the NIH HD007333 Developmental Psychobiology and Neurobiology Training Grant. AJL acknowledges support from NSF-DMR-0907212. G. P. acknowledges stimulating discussions with Tommy Angelini.